

Two *Drosophila* Myosin Transducer Mutants with Distinct Cardiomyopathies Have Divergent ADP and Actin Affinities*

Received for publication, May 9, 2011, and in revised form, June 15, 2011. Published, JBC Papers in Press, June 16, 2011, DOI 10.1074/jbc.M111.258228

Marieke J. Bloemink[‡], Girish C. Melkani[§], Corey M. Dambacher^{§1}, Sanford I. Bernstein^{§2}, and Michael A. Geeves^{‡3}

From the [‡]Department of Biosciences, University of Kent, Canterbury, Kent CT2 7NJ, United Kingdom and the [§]Department of Biology and Molecular Biology Institute, San Diego State University, San Diego, California 92182-4614

Two *Drosophila* myosin II point mutations (*D45* and *Mhc*⁵) generate *Drosophila* cardiac phenotypes that are similar to dilated or restrictive human cardiomyopathies. Our homology models suggest that the mutations (A261T in *D45*, G200D in *Mhc*⁵) could stabilize (*D45*) or destabilize (*Mhc*⁵) loop 1 of myosin, a region known to influence ADP release. To gain insight into the molecular mechanism that causes the cardiomyopathic phenotypes to develop, we determined whether the kinetic properties of the mutant molecules have been altered. We used myosin subfragment 1 (S1) carrying either of the two mutations (S1^{A261T} and S1^{G200D}) from the indirect flight muscles of *Drosophila*. The kinetic data show that the two point mutations have an opposite effect on the enzymatic activity of S1. S1^{A261T} is less active (reduced ATPase, higher ADP affinity for S1 and actomyosin subfragment 1 (actin·S1), and reduced ATP-induced dissociation of actin·S1), whereas S1^{G200D} shows increased enzymatic activity (enhanced ATPase, reduced ADP affinity for both S1 and actin·S1). The opposite changes in the myosin properties are consistent with the induced cardiac phenotypes for S1^{A261T} (dilated) and S1^{G200D} (restrictive). Our results provide novel insights into the molecular mechanisms that cause different cardiomyopathy phenotypes for these mutants. In addition, we report that S1^{A261T} weakens the affinity of S1·ADP for actin, whereas S1^{G200D} increases it. This may account for the suppression (A261T) or enhancement (G200D) of the skeletal muscle hypercontraction phenotype induced by the troponin I *held-up*² mutation in *Drosophila*.

Myosins are a large family of actin-based molecular motor proteins, of which at least 35 different classes are known (1). They show a wide variety of different mechanical activities, such as muscle contraction, phagocytosis, cell motility, tension maintenance, and vesicle transport (2). Striated muscle myosin is a class II molecular motor and consists of two myosin heavy chains (MHC), two essential light chains, and two regulatory

light chains. Muscle contraction results from cyclic interactions between myosin II motors and actin filaments, also known as the cross-bridge cycle. These force-generating interactions are driven by the hydrolysis of ATP at the myosin active site (3). Mutations in human myosin II domains have been associated with both skeletal and cardiac myopathies (4).

Drosophila melanogaster has been described as a useful model system to study cardiomyopathies (5, 6). A recent study of myosin heavy chain mutations in *Drosophila* has shown that two mutations in the myosin motor domain generate defects in the *Drosophila* heart. The mutation known as *D45*⁴ (point mutation A261T) has a phenotype similar to human dilated cardiomyopathy (DCM),⁵ whereas *Mhc*⁵ (point mutation G200D) has a restrictive cardiomyopathy phenotype (RCM, a subset of hypertrophic cardiomyopathies (HCMs)) (7). The two myosin mutations identified are localized in the transducer region (Fig. 1), which is encoded by constitutive exons of the alternatively spliced *Mhc* transcript. *D45* (A261T) is located on one of the β -strands (β^7) close to the β -bulge between β^6 and β^7 , whereas *Mhc*⁵ (G200D) is at the N-terminal side of loop 1 (using chicken skeletal myosin residue numbers as introduced by Kronert *et al.* (8); the analogous *Drosophila* residues are Gly²⁰⁰ and Ala²⁵⁸). The transducer region is thought to integrate the structural changes from different parts of the motor domain and includes the seven-stranded β -sheet plus various flexible elements such as loop 1, the β -bulge between β^6 and β^7 , the HO-linker, and the nucleotide-sensing elements such as the phosphate binding loop (P-loop), switch-1, and switch-2 (11). The seven-stranded β -sheet becomes distorted when myosin switches between the rigor-like and post-rigor states, and this distortion is facilitated by the flexible elements.

In an earlier study, *D45* and *Mhc*⁵ were shown to interact with a mutation in troponin I (*held-up*² (*hdp*²)) that causes hypercontractility of the indirect flight muscle (IFM) (8). *D45* is a suppressor of the TnI mutation (A116V) in the IFM, and in *Drosophila* hearts, it leads to a DCM-like phenotype in the presence of normal troponin I, whereas *Mhc*⁵ leads to RCM in the

* This work was supported, in whole or in part, by National Institutes of Health Research Grant GM32443 (to G. C. M., C. M. D., and S. I. B.). This work was also supported by Wellcome Trust Program Grant 085309 (to M. A. G. and M. J. B.).

⌘ Author's Choice—Final version full access.

¹ Present address: The Scripps Research Institute, Dept. of Chemistry and Skaggs Institute for Chemical Biology, 10550 N. Torrey Pines Rd., SR207, La Jolla, CA 92037.

² To whom correspondence may be addressed. E-mail: sbernst@sciences.sdsu.edu.

³ To whom correspondence may be addressed. E-mail: m.a.geeves@kent.ac.uk.

⁴ The two mutants used throughout this study are: *Mhc*⁵, which indicates the myosin heavy chain mutation G200D; and *D45*, which indicates the myosin heavy chain mutation A261T.

⁵ The abbreviations used are: DCM, dilated cardiomyopathy; HCM, hypertrophic cardiomyopathy; RCM, restrictive cardiomyopathy; S1, myosin subfragment 1; actin·S1, actomyosin subfragment 1; cATP, caged ATP; cADP, caged ADP; eda-deac-ATP, 3'-O-[N-[2-(7-diethylamino-coumarin-3-carboxamido)ethyl]carbonyl]-ATP; eda-deac-ADP, 3'-O-[N-[2-(7-diethylamino-coumarin-3-carboxamido)ethyl]carbonyl]-ADP; IFI, indirect flight muscle isoform; IFM, indirect flight muscle; Tn, troponin; TnI, troponin I; EMB, embryonic myosin S1.

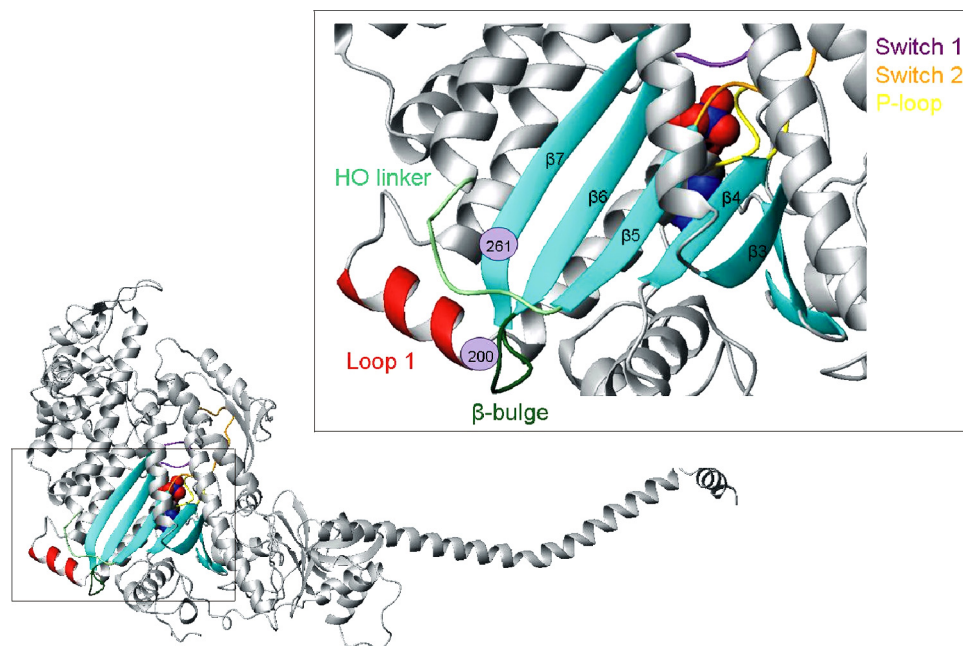


FIGURE 1. Location of the transducer in the myosin motor domain of *Drosophila*. Shown is a homology model of *Drosophila* myosin S1 built using the crystal structure of scallop myosin (pre-powerstroke conformation) as a template (PDB code 1qvi). The transducer region in the myosin head of *Drosophila* is indicated and expanded in a separate panel. The locations of the two point mutations, S1^{G200D} and S1^{A261T}, are indicated (purple circles), and the position of the nucleotide (space-filling model) is also shown.

heart and is lethal in combination with *hdp*². This suggests the likelihood of opposite effects of the two myosin mutations in regard to TnI interaction and that such differential activity may lead to the observed alternative cardiomyopathies.

Although a large number of human cardiomyopathies have been linked with specific mutations in sarcomeric proteins, including myosins, the causal relationship is not well understood. For mutations in the thin filament proteins tropomyosin (Tm) and troponin (Tn), there is an emerging paradigm that mutations that increase calcium sensitivity of the thin filament regulation of contraction result in HCM, whereas a decrease in calcium sensitivity is associated with DCM (9, 10). Because the *held-up*² TnI mutation leads to over-contraction, the myosin mutation may reduce calcium sensitivity (*D45*) to compensate for the TnI mutation or increase it further (*Mhc*⁵) to cause lethality. Indeed, *Drosophila D45* myosin has reduced ATPase activity and reduced *in vitro* motility, whereas *Mhc*⁵ myosin displays an increase in both ATPase activity and *in vitro* motility (7). It was argued that this is consistent with *D45* suppressing the TnI mutation and *Mhc*⁵ enhancing it. However, the molecular mechanism for this interaction remains to be explored.

In this study, we used myosin subfragment 1 (S1) to investigate the transient and steady-state kinetics of the two transducer mutants of myosin S1 that suppress (A261T) or enhance (G200D) the TnI defect (A116V). We will use S1^{A261T} and S1^{G200D} nomenclature for the two mutants throughout this study, and the properties and nomenclature of these mutants are summarized in Table 1. The kinetic data show that the two point mutations have an opposite effect on the enzymatic activity of S1 myosin as compared with wild type, resulting in a less active myosin (S1^{A261T}) or more active myosin (S1^{G200D}). These observations are consistent with the induced cardiac

TABLE 1

Overview of the two *Drosophila* myosin transducer mutants

	<i>Mhc</i> ⁵	<i>D45</i>
Point mutation	G200D	A261T
Location in transducer	Loop 1	β7
Interaction with flightless TnI (A116V) <i>held-up</i> ² allele	Lethal	Rescued
<i>Drosophila</i> cardiac phenotype	RCM	DCM

phenotypes for the two mutants. In addition, we report that the two mutations change the affinity of S1•ADP for actin in opposite directions and that these changes can account for the differential interaction of the two mutations with the TnI *held-up*² mutation in *Drosophila*.

EXPERIMENTAL PROCEDURES

Myosin Isolation and Generation of Its S1—Myosin was isolated from IFM of less than 1-day-old wild-type and *D45*(A261T) or *Mhc*⁵(G200D) mutant flies as described previously (12). The original procedure has been modified so that all dilutions were carried out with water containing 10 mM DTT and all solution volumes were reduced to 75% (7). Digestion of the S1 subfragment was carried out with chymotrypsin as described previously (13–15) with the following modifications. The final myosin pellet obtained after centrifugation was resuspended in digestion buffer (120 mM NaCl, 20 mM Na₂PO₄, pH 7.0, 1 mM EDTA, and 20 mM DTT). Samples were incubated on ice for ~6 min. The myosin solution was then placed in a 20 °C water bath for 5 min for temperature equilibration. The addition of α-chymotrypsin (0.2 mg/ml final concentration from 10 mg/ml stock solution) to the myosin solution was carried out in the 20 °C water bath followed by incubation for 6 min. To quench the reaction, 1.5 mM (final concentration) of phenylmethylsulfonyl fluoride (PMSF) was added. To pellet undigested myosin or myosin rod, the sample was immediately cen-

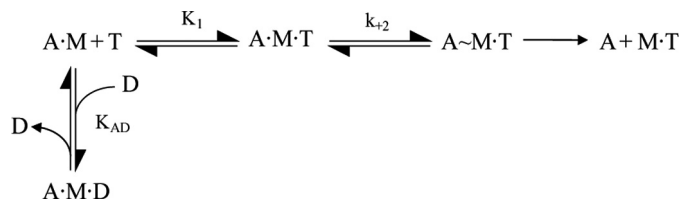
trifuged at 68,000 rpm ($250,000 \times g$, TLA 100.3 rotor) for 30 min in a Beckman ultracentrifuge. The supernatant was removed and diluted 10-fold with low salt buffer (30 mM KCl, 5 mM MgCl₂, 20 mM MOPS, pH 7.0, and 4 mM DTT) and incubated for 30 min on ice. Any remaining uncut myosin or rod contamination was eliminated by centrifugation at 68,000 rpm for 20 min. For S1 concentration, the samples were centrifuged at $12,000 \times g$ in a Sorvall MC 12 V at 4 °C using a Millipore Ultrafree 0.5- μ m centrifugal Biomax-5 filter with a 5-kDa cut-off. The final volume of the supernatant was 40–60 μ l. S1 concentration was determined from A_{280} ($= 0.75 \text{ cm}^{-1}$ for 1 mg of S1 per ml) and a molecular mass of 115 kDa. A single band of S1 was detected on SDS polyacrylamide gels for all samples. All steady-state kinetic measurements were performed with freshly prepared S1, and transient kinetics experiments were performed within 1 week after S1 preparation.

G- and F-actin Preparation—G-actin was isolated from acetone powder of chicken skeletal muscle as described previously (1–4). After multiple cycles of polymerization-depolymerization, soluble G-actin was obtained after dialysis against 2 mM Tris-Cl (pH 8), 0.2 mM ATP, 2 mM CaCl₂, and 1 mM DTT and quantified spectrophotometrically using an extinction coefficient of 0.62 cm^{-1} ($A_{310 \text{ nm}} - A_{290 \text{ nm}}$) for 1 mg of actin ml⁻¹. To obtain a G-actin solution of 150–250 μ M, the G-actin solution was concentrated using a Millipore Biomax-5 filter as described above. F-actin was prepared by adding 1 volume of $10 \times$ polymerization buffer (50 mM Tris-Cl, pH 8, 0.5 M KCl, 20 mM MgCl₂, and 10 mM ATP) to 9 volumes of G-actin. Actin was stored on ice at 4 °C and used within 1 month of preparation for actin-activated Mg²⁺-ATPase assays.

Steady-state ATPase Activity—ATPase activities were determined using [γ -³²P]ATP as described previously in detail for full-length myosin (7). Ca²⁺ ATPase was carried out as per full-length myosin, but basal Mg²⁺ and actin-activated Mg²⁺-ATPase procedures involved some modifications. Briefly, 2 μ g of S1 were added to Mg-ATPase solution without KCl (10 mM imidazole, 0.1 mM CaCl₂, 1 mM MgCl₂, 1 mM [γ -³²P]ATP), in the absence or in the presence of increasing concentrations of F-actin. After 30 min at room temperature (21–23 °C), the reaction was quenched using 1.8 N HClO₄. Extraction and scintillation counting were carried out essentially as for full-length myosin (7, 13). Basal Mg²⁺-ATPase activities obtained in the absence of actin were subtracted from all data points. Actin-activated V_{max} and K_m values for actin were obtained by fitting all data points from several preparations of wild-type or mutant S1 with the Michaelis-Menten equation using SigmaPlot. Values were averaged to give mean \pm S.D. Statistical differences of Ca²⁺ ATPase, Mg²⁺ ATPase, V_{max} , and K_m between wild-type and mutant S1 were carried out using Student's *t* tests.

Chemicals—Caged ATP (cATP) was purchased from Molecular Probes. Coumarin-labeled ATP (3'-O-{N-[2-(7-diethylamino-coumarin-3-carboxamido)ethyl]carbonyl}-ATP, abbreviated to eda-deac-ATP) was a gift from Martin Webb (National Institute for Medical Research, Mill Hill, London, UK) and was prepared for use in the transient kinetic studies according to methods described previously (16, 17).

Flash Photolysis System—Due to the small amount of protein available and the relatively poor fluorescence signal changes



SCHEME 1. The interaction of S1 with actin, ATP and ADP. M, A, T, and D symbolize S1, actin, ATP, and ADP, respectively.

observed with pyrene-labeled actin, flash photolysis was the method of choice to investigate the kinetic properties of the *Drosophila* myosin S1 proteins (18). The ATP-induced dissociation of the actin·S1 complex changes the light-scattering signal, and the dissociation of nucleotide from S1 was followed by fluorescence changes. All light-scattering experiments were conducted in a low salt buffer (pH 7.0: 30 mM KCl, 5 mM MgCl₂, 20 mM MOPS, and 10 mM DTT, 20 °C) with 1 μ M actin, 1–3 μ M S1, and 500 μ M cATP. eda-deac-ADP dissociation experiments were also performed in this low salt buffer and contained 4 μ M S1, 10 μ M eda-deac-ATP (source of eda-deac-ADP), and 100 μ M cATP (S1^{A261T}) or caged ADP (cADP) (S1^{G200D}).

Analysis of Transient Kinetic Data—The following equation was derived from the interaction of actin and S1 with ATP and ADP shown in Scheme 1 and was used to determine K_{AD}

$$k_{\text{obs}} = K_1 k_{+2} ([\text{ATP}] / (1 + [\text{ADP}] / K_{AD})) \quad (\text{Eq. 1})$$

where k_{obs} is the observed rate constant for the ATP-induced dissociation of actin·S1; $K_1 k_{+2}$ is the second-order rate constant for ATP binding to actin·S1; and K_{AD} is the equilibrium dissociation constant for the binding of ADP to actin·S1. The equation $k_{\text{rel}} = k_{\text{obs}} / k_0$ was used to determine the relative rate constant (k_{rel}) shown in Fig. 5, where k_0 is the value when $[\text{ADP}] = 0$.

Co-sedimentation Assay—Co-sedimentation assays were done as described previously with some minor modifications (14). S1 (100 nM) was incubated with increasing actin concentrations (0–500 nM) in low salt buffer (30 mM KCl, 5 mM MgCl₂, 20 mM MOPS, pH 7.0, and 4 mM DTT) with a total volume of 100 μ l and then centrifuged at $400,000 \times g$ for 30 min at low temperature (4 °C) to determine K_A . Measurements were repeated in the presence of 10 mM ADP with 500 nM S1 and increasing actin concentrations (0–5 μ M) to determine K_{DA} . The supernatant was separated from the pellet at each actin concentration, and the pellets were resuspended in 100 μ l of water. All samples were applied to a 10% SDS-polyacrylamide gel. The density of each protein band was quantified and used to determine the affinity of S1 for actin as described previously (14).

Homology Models—Homology models of the wild-type indirect flight muscle isoform (IFI) and the two point mutants S1^{A261T} and S1^{G200D} were built as described using SWISS-MODEL (19). When aligning the IFI myosin head sequence with class II scallop myosin, the sequence identity is $60 \pm 1\%$, enabling us to build well resolved homology models (20). Crystal structures of the various states of scallop myosin during the cross-bridge cycle were chosen to generate three-dimensional homology models of IFI, S1^{A261T}, and S1^{G200D}: the near-rigor state of myosin (Protein Data Bank (PDB) code 1sr6), the post-

Point Mutants of *Drosophila* Muscle Myosin

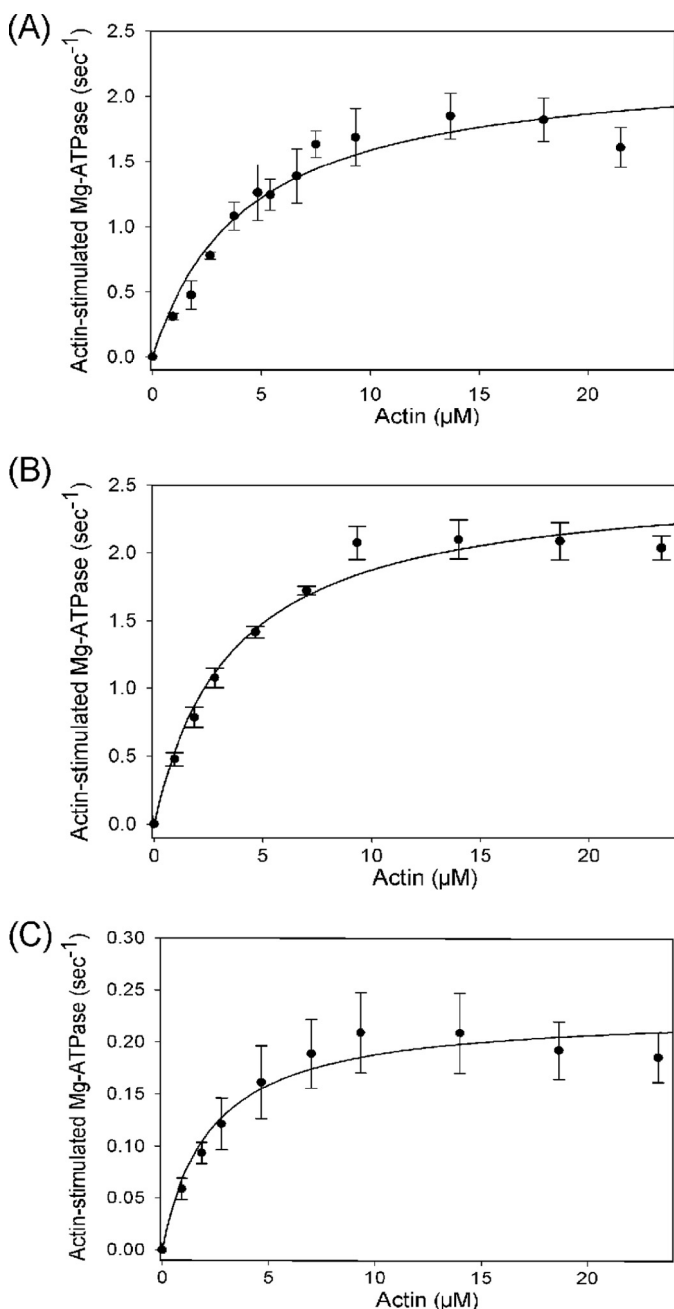


FIGURE 2. Actin-stimulated ATPase activity of wild-type IFI (A), S1^{G200D} (B), and S1^{A261T} (C). Basal Mg²⁺-ATPase and actin-stimulated Mg²⁺-ATPase data were obtained in the absence or in the presence of increasing concentrations of actin as described under "Experimental Procedures." To obtain K_m and V_{max} , basal Mg-ATPase values were subtracted from actin-activated ATPase values, and data points were fit to a hyperbola. Statistical significance of data comparisons are shown in Table 2.

TABLE 2

Steady-state kinetic parameters measured for wild-type, G200D and A261T *Drosophila* myosin S1

Values are mean \pm S.D. based on a minimum of four preparations.

Myosin S1	Basal Ca-ATPase s^{-1}	Basal Mg-ATPase s^{-1}	V_{max} s^{-1}	K_m μM	V_{max}/K_m $\mu M^{-1} s^{-1}$
Wild-type IFI	5.33 ± 0.62	0.09 ± 0.01	2.54 ± 0.29	5.77 ± 0.83	0.45 ± 0.09
S1 ^{G200D} (<i>Mhc</i> ^c)	5.36 ± 0.27	0.14 ± 0.01^a	2.60 ± 0.18	3.79 ± 0.67^b	0.70 ± 0.08^b
S1 ^{A261T} (<i>D45</i>)	1.97 ± 0.46^a	0.04 ± 0.01^a	0.23 ± 0.04^a	2.15 ± 0.73^a	0.11 ± 0.02^a

^a $p < 0.001$ determined by Student's t test as compared with IFI.

^b $p < 0.01$ determined by Student's t test as compared with IFI.

rigor actin-detached state (PDB code 1kk8) that contains ADP·BeF_x, the pre-powerstroke state (PDB code 1qvi) that contains ADP·VO₄, and a novel conformation that contains partially bound ADP·SO₄ (PDB code 1s5g). For regions of insertions or deletions in the target-template alignment, SWISS-MODEL constructs an ensemble of fragments compatible with the neighboring stems using constraint space programming or a loop library (20, 21).

RESULTS

Catalytic Activity Is Reduced for S1^{A261T} and Increased for S1^{G200D}—The basal and actin-activated Mg²⁺-ATPase activities of wild-type myosin S1 and the two point mutants (S1^{A261T} and S1^{G200D}) were measured (Fig. 2), and the results are summarized in Table 2. The TnI *hdp*² suppressor mutant S1^{A261T} showed a more than 2-fold reduction in basal Mg²⁺-ATPase activity ($0.04 s^{-1}$), a nearly 3-fold reduction in basal Ca²⁺-ATPase ($1.97 s^{-1}$), and a 10-fold reduction in V_{max} ($0.23 s^{-1}$) as compared with wild type (0.09 , 5.33 , and $2.54 s^{-1}$, respectively) (difference significance at <0.001 in each case). In contrast, the *hdp*² enhancer mutant S1^{G200D} showed nearly a 2-fold increase in basal Mg²⁺-ATPase ($0.14 s^{-1}$) and no significant change in basal Ca²⁺-ATPase or V_{max} .

The earlier ATPase measurements for full-length myosin (7) cannot be compared directly with the S1 ATPases described here because the two assays use different salt concentrations and the filamentous two-headed full-length myosin has a different affinity for actin than the soluble S1. However, the relative effects of the mutations on the S1 and the full-length myosin basal Mg²⁺-ATPases and the V_{max} are similar (full-length myosin basal Mg²⁺-ATPase, 0.2 , 0.48 , and $0.11 s^{-1}$, and V_{max} of 1.8 , 1.5 , and $0.69 s^{-1}$ for wild type, G200D, and A261T, respectively). The K_m for actin with the S1 constructs of either S1^{A261T} ($K_m = 2.15 \mu M$) or S1^{G200D} ($K_m = 3.79 \mu M$) showed a decrease relative to wild type ($K_m = 5.77 \mu M$), which was not seen previously with full-length myosin. The ratio V_{max}/K_m , referred to as the catalytic efficiency, shows a significant ($p < 0.01$) increase for S1^{G200D} ($0.70 \mu M^{-1} s^{-1}$) as compared with wild type ($0.45 \mu M^{-1} s^{-1}$), whereas for S1^{A261T}, this ratio decreases 4-fold ($0.11 \mu M^{-1} s^{-1}$, significance $p < 0.001$). Using flash photolysis, the turnover number (k_{cat}) was measured at a fixed actin concentration ($2 \mu M$) for the point mutants S1^{G200D} and S1^{A261T} and compared with wild type (Fig. 3). The catalytic activity of S1^{A261T} ($k_{cat} = 0.064 s^{-1}$) is reduced as compared with wild type ($0.172 s^{-1}$), whereas k_{cat} of S1^{G200D} ($0.210 s^{-1}$) is increased. This demonstrates that the differences seen in the lower ionic strength ATPase assay above remain at the higher salt concentrations ($30 mM KCl$) used for the transient kinetic measurements.

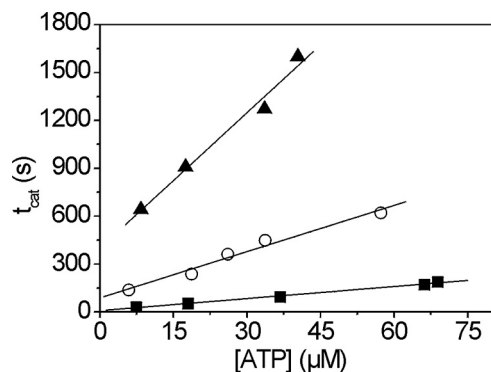


FIGURE 3. The turnover number (k_{cat}) for actin-S1 of point mutants $S1^{G200D}$ and $S1^{A261T}$ as compared with wild-type IFI S1. Light-scattering transients monitoring dissociation of the acto-S1 complex ($2 \mu\text{M}$) and subsequent reassociation were measured using varying amounts of ATP. The time taken to hydrolyze all ATP (t_{cat}) was linearly dependent upon the amount of released ATP. The steady-state rate of ATP hydrolysis can be determined from the inverse of the slope (steady-state rate = $[\text{ATP}]/t_{cat}$), allowing the determination of the catalytic activity. The catalytic activity of $S1^{A261T}$ (0.064 s^{-1}) (\blacktriangle) is significantly reduced as compared with wild-type S1 (0.172 s^{-1}) (\circ) and slightly increased for $S1^{G200D}$ (0.210 s^{-1}) (\blacksquare).

ATP-induced Dissociation of Actin-S1 Is Slower for $S1^{A261T}$ but Unaltered for $S1^{G200D}$ —The second-order rate constant governing the dissociation of acto-S1 by ATP (K_1k_{+2} ; see Scheme 1) was measured as described previously (14). Briefly, $1 \mu\text{M}$ actin and $1\text{--}3 \mu\text{M}$ S1 were preincubated and then dissociated by ATP released from cATP. In the presence of apyrase, a single sample was subjected to a series of laser flashes decreasing in intensity to release varying concentrations of ATP. The rate of change in light scattering was recorded for each laser flash and could be well described by a single exponential at each ATP concentration (Fig. 4, A and B). The slope of a graph of k_{obs} versus ATP concentration determines the apparent second-order rate constant K_1k_{+2} for the dissociation of actin-S1 by ATP (Fig. 4C). As compared with the value for wild type ($0.75 \mu\text{M}^{-1} \text{ s}^{-1}$), $S1^{A261T}$ showed a reduced ATP-induced dissociation rate ($0.47 \mu\text{M}^{-1} \text{ s}^{-1}$), whereas the rate measured for $S1^{G200D}$ ($0.64 \mu\text{M}^{-1} \text{ s}^{-1}$) was similar to wild type (Table 3).

Affinity of Actin-S1 for ADP Is Weak for $S1^{G200D}$ but Strong for $S1^{A261T}$ —The ADP affinity for S1 in the presence of actin, defined by the equilibrium dissociation constant K_{AD} , was determined as described previously (14). In the presence of increasing concentrations of ADP, the ATP-induced dissociation of actin-S1 was measured using light scattering, and plotting the relative k_{obs} (k_{rel}) versus ADP concentration allows the measurement of the ADP affinity K_{AD} for actin-S1 (Fig. 5 and Scheme 1). The K_{AD} of $S1^{A261T}$ ($K_{AD} = 293 \mu\text{M}$) is reduced by almost 30% as compared with wild type ($K_{AD} = 409 \mu\text{M}$), whereas for $S1^{G200D}$, the K_{AD} value is increased ($K_{AD} = 604 \mu\text{M}$) (Fig. 5 and Table 3). Thus the ADP affinity of the two point mutants is affected in opposing ways with $S1^{G200D}$ having a weaker ADP affinity and $S1^{A261T}$ displaying a stronger ADP affinity as compared with wild type.

ADP Release from S1 (k_{-D}) Is Fast for $S1^{G200D}$ but Slow for $S1^{A261T}$ —To estimate the rate constant of ADP dissociation from S1 in the absence of actin, the change in fluorescence of coumarin-labeled ADP (eda-deac-ADP) was measured upon displacement of eda-deac-ADP by ATP binding to S1. It was

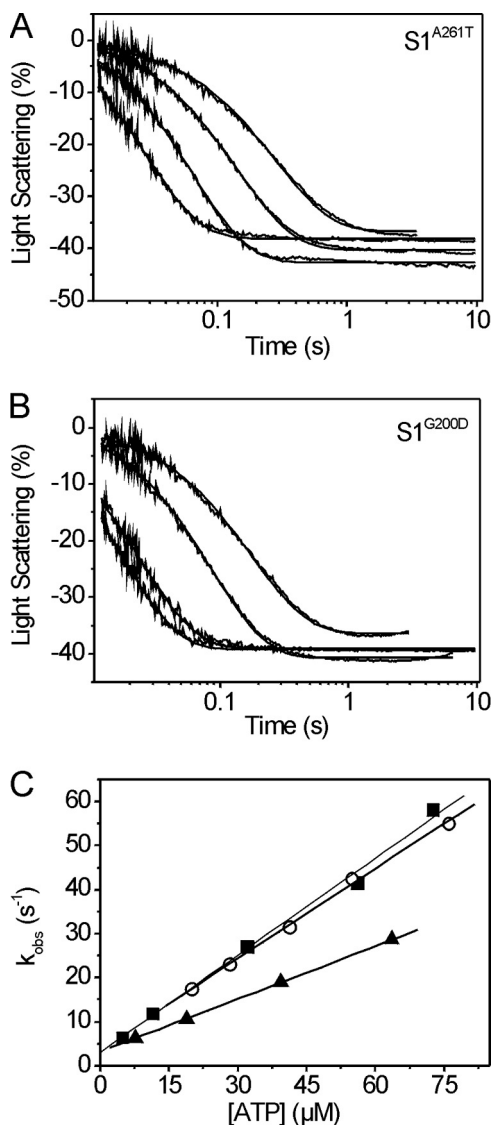


FIGURE 4. ATP-induced dissociation rate (K_1k_{+2}) of $S1^{G200D}$ and $S1^{A261T}$. A and B, light-scattering transients monitoring dissociation of the actin-S1 complex ($1 \mu\text{M}$ phalloidin-stabilized actin and $1\text{--}3 \mu\text{M}$ S1) after release of ATP from caged ATP. The traces measured for $S1^{A261T}$ (A) or $S1^{G200D}$ (B) were fitted with a single exponential at each ATP concentration to determine the k_{obs} . C, the second-order rate constant for the dissociation of S1 from actin is determined from a linear fit to the plot of the k_{obs} versus $[\text{ATP}]$, resulting in values of $0.47 \pm 0.08 \mu\text{M}^{-1} \text{ s}^{-1}$ for $S1^{A261T}$ (\blacktriangle) and $0.64 \pm 0.09 \mu\text{M}^{-1} \text{ s}^{-1}$ for $S1^{G200D}$ (\blacksquare) as compared with $0.75 \pm 0.08 \mu\text{M}^{-1} \text{ s}^{-1}$ for wild-type IFI (\circ).

shown previously that this coumarin-labeled analog has very similar kinetic properties as compared with ADP (17). Measuring the ADP release rate (k_{-D}) for wild type and $S1^{A261T}$ was relatively straightforward. A single laser flash released $15\text{--}20 \mu\text{M}$ ATP from cATP ($100 \mu\text{M}$), and the fluorescence change resulting from eda-deac-ADP release is well described by a single exponential function, as shown in Fig. 6A. The observed rate constant for ADP release ($k_{-D} = 4.1 \text{ s}^{-1}$) was slower as compared with wild type ($k_{-D} = 7.3 \text{ s}^{-1}$).

For $S1^{G200D}$, a different approach was needed because it was noted that the fluorescence signal of the sample containing $S1^{G200D}$ increased on adding cATP, indicating that cATP could displace eda-deac-ADP for this mutant. This displacement of eda-deac-ADP by cATP was not seen for wild-type S1, indicat-

TABLE 3

Transient kinetic parameters measured for wild-type, G200D and A261T *Drosophila* myosin S1

Values are mean \pm S.D. based on a minimum of three preparations (two preparations in the case of K_{DA}). K_1k_{+2} is the second-order rate constant for ATP-induced dissociation of actin-S1. K_D and K_{AD} are ADP dissociation equilibrium constants. k_{-D} and k_{-AD} are the ADP dissociation rate constants in the absence and presence of actin, respectively (note that $K_D = k_{-D}/k_{+D}$). K_{AD}/K_D is the thermodynamic coupling constant describing the relationship between actin and ADP affinities. K_{DA} = actin affinity of S1-ADP.

Myosin S1	K_1k_{+2} $\mu\text{M}^{-1} \text{s}^{-1}$	K_{AD} μM	k_{-AD} ^a s^{-1}	k_{-D} s^{-1}	K_D ^b μM	K_{AD}/K_D	K_{DA} nM
Wild-type IFI	0.75 ± 0.08^c	409 ± 26^c	4090	7.5 ± 1.3^c	7.5	54	446 ± 125
S1 ^{G200D} (Mhc ⁵)	0.64 ± 0.09^d	604 ± 157^d	6040	71 ± 19^e	71	8.5	62 ± 12^d
S1 ^{A261T} (D45)	0.47 ± 0.08^e	293 ± 61^e	2930	4.1 ± 0.3^e	4.1	71	684 ± 240^d

^a Data are estimated from K_{AD} assuming an association rate constant of $10^7 \text{ M}^{-1} \text{ s}^{-1}$.

^b Data are estimated from k_{-D} assuming an association rate constant of $10^6 \text{ M}^{-1} \text{ s}^{-1}$.

^c Data are from Miller *et al.* (14).

^d $p < 0.05$ determined by Student's *t* test as compared with IFI.

^e $p < 0.01$ determined by Student's *t* test as compared with IFI.

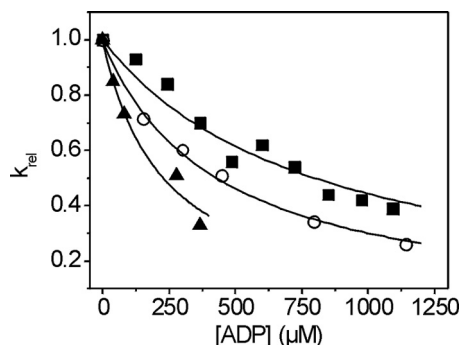


FIGURE 5. **The affinity of ADP (K_{AD}) for actin-S1.** The dissociation of actin-S1 was induced by ATP in the presence of ADP ranging from 0 to 1200 μM . The light-scattering traces were fitted with single exponentials to determine the k_{obs} . Hyperbolic plots of the k_{rel} (k_{obs}/k_0) versus ADP concentration were fitted with an equation derived from Scheme 1 ($k_{\text{obs}} = K_1k_{+2}([\text{ATP}]/(1 + [\text{ADP}]/K_{AD}))$) to determine K_{AD} . The fits yielded a value of $293 \pm 61 \mu\text{M}$ for S1^{A261T} (\blacktriangle) and $604 \pm 157 \mu\text{M}$ for S1^{G200D} (\blacksquare) as compared with $409 \pm 26 \mu\text{M}$ for wild-type IFI (\circ).

ing that the ADP affinity of S1^{G200D} is much weaker. Using cADP instead of cATP to displace eda-deac-ADP from S1 resolved this problem because cADP has a much weaker affinity for myosin S1 (22). No fluorescence signal change was observed when adding cADP to S1 (incubated with eda-deac-ADP) prior to applying the laser flash. However, after release of ADP ($\sim 200 \mu\text{M}$) from cADP (1000 μM), the eda-deac-ADP fluorescence increased on displacement (Fig. 6B) with a nearly 10-fold increase in rate constant for ADP release from S1^{G200D} ($k_{-D} = 71 \text{ s}^{-1}$) as compared with wild type.

With S1^{A261T}, the eda-deac-ADP fluorescence decreased on displacement by ATP, which is the same direction as for wild type and for other *Drosophila* myosin isoforms, such as embryonic myosin S1 (EMB) (14, 15). The results with S1^{G200D} showed a fluorescence increase upon eda-deac-ADP displacement, as was found previously for the *Drosophila* chimeric constructs EMB-7d/7a and IFI-7a (19) and EMB-9a and IFI-9b (15). Similar variation in the direction of fluorescence changes has been observed previously with vertebrate and *Dictyostelium* S1 isoforms (22), and no correlation was found between the direction of the fluorescence change and the affinity of the analog for S1. The variation in signal direction reflects differences in the local environment of the protein-bound fluorophore; therefore the G200D mutation does change the local environment sensed by the coumarin fluorophore.

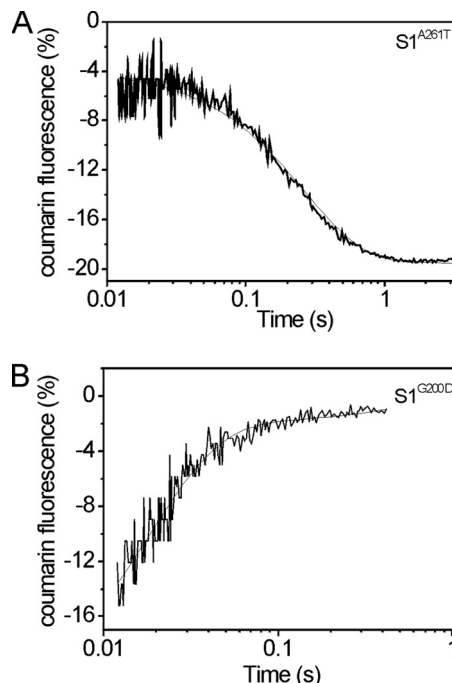


FIGURE 6. **Rate of eda-deac-ADP dissociation (k_{-D}) from *Drosophila* point mutant S1^{A261T} (A) and S1^{G200D} (B).** A, fluorescence signal after releasing ATP (15 μM) from caged ATP (100 μM) by a single laser flash displacing the eda-deac-ADP bound to S1^{A261T}. Fitting with a single exponential resulted in $k_{-D} = 4.1 \pm 0.3 \text{ s}^{-1}$. B, fluorescence signal after release of ADP ($\sim 200 \mu\text{M}$) from cADP (1000 μM) by a single laser flash displacing eda-deac-ADP from S1^{G200D}. Fitting with a single exponential resulted in $k_{-D} = 71 \pm 19 \text{ s}^{-1}$.

Affinity of S1 for Actin in the Presence of ADP Is Weak for S1^{A261T} but Strong for S1^{G200D}—The measurement of the affinity of S1 and actin-S1 for ADP (K_D and K_{AD}) allows us to calculate the thermodynamic coupling constant (K_{AD}/K_D) for the interaction between the actin and ADP sites on S1. This ratio of two independent values carries a large error and includes the assumption that k_{+AD} has the same value for all constructs. The values listed in Table 3 are shown for illustration, acknowledging the error. The numbers do show a 6-fold reduction for G200D in the coupling (from 54 for wild type to 8.5 for the mutation). In contrast, A261T has a 30% increase in coupling ($K_{AD}/K_D = 71$), which is not very different from the 20% error of the K_{AD} value. Here we can use the values to predict the effect of ADP on the affinity of S1 for actin for the two mutants. In our earlier work (14), we estimated that the affinity of wild-type S1 for actin (K_A) was $\leq 10 \text{ nM}$. Assuming that the affinity of S1 for

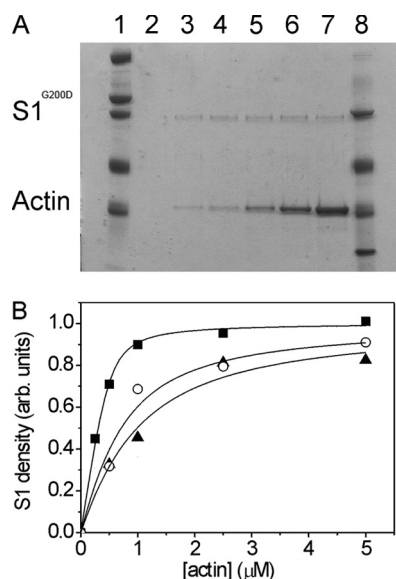


FIGURE 7. Determination of actin affinity in the presence of ADP (24). The affinity of S1 for actin was characterized with the co-sedimentation method (see "Experimental Procedures"). *A*, representative SDS-polyacrylamide gel of the pellets from experiments where $S1^{G200D}$ (100 nM) was mixed with various actin concentrations (0, 0.25, 0.5, 1.0, 2.5, and 5 μM (lanes 2, 3, 4, 5, 6, and 7, respectively)) in the presence of ADP (10 mM). Lanes 1 and 8 contain molecular weight markers. *B*, the densities of the myosin S1 bands as a function of [actin] shown for wild-type IFI (\circ) and the two point mutants $S1^{G200D}$ (\blacksquare) and $S1^{A261T}$ (\blacktriangle). The fits for these samples gave a value of $K_{DA} = 62$ nM ($S1^{G200D}$), $K_{DA} = 684$ nM ($S1^{A261T}$), and $K_{DA} = 446$ nM (IFI-WT). *arb. units*, arbitrary units.

actin remains very tight and is relatively little affected by mutations that are remote from the actin binding site, then K_{DA} can be estimated from $K_{AD}/K_D = K_{DA}/K_A$, where K_{DA} is the affinity of S1 for actin in the presence of ADP. This estimates K_{DA} as ≤ 540 nM for wild type and ≤ 710 and 85 nM for A261T and G200D, respectively. Using the co-sedimentation assay of Miller *et al.* (14), we found that the affinity of S1 for actin did remain very tight for the mutant S1s. The value of K_{DA} was measured as shown in Fig. 7, giving values of 446 nM for wild type, a weaker affinity of 684 nM for A261T, and a significantly tighter affinity of 62 nM for G200D (Table 3). Although the precision of these measurements is not high for this type of assay, the values are in line with the predictions.

Homology Models Suggest a Role for Loop 1—Homology models were built of wild type and mutants $S1^{G200D}$ and $S1^{A261T}$ to help understand the mechanism of action of the mutated residues. Fig. 8 shows part of the transducer area of the homology structures representing the pre-powerstroke state, and in particular, loop 1. The model of $S1^{A261T}$ suggests a helical structure for loop 1 (*panel B*), as is also found in the homology model for wild type (*panel A*). For $S1^{A261T}$, however, the model indicates a possible hydrogen bond between the side chains of Thr²⁶¹ and the conserved loop 1 residue Lys²⁰³ (which is absent in wild-type S1, which has Ala²⁶¹). This interaction could affect the flexibility of loop 1, resulting in a more stable loop 1 structure and thus slower nucleotide binding or release from the nucleotide binding pocket. For $S1^{G200D}$, the homology model suggests a less ordered loop 1 structure as compared with wild type (*panel A*), enhancing its flexibility, which ultimately could affect nucleotide exchange. For the other conformational states, the differences between the three constructs

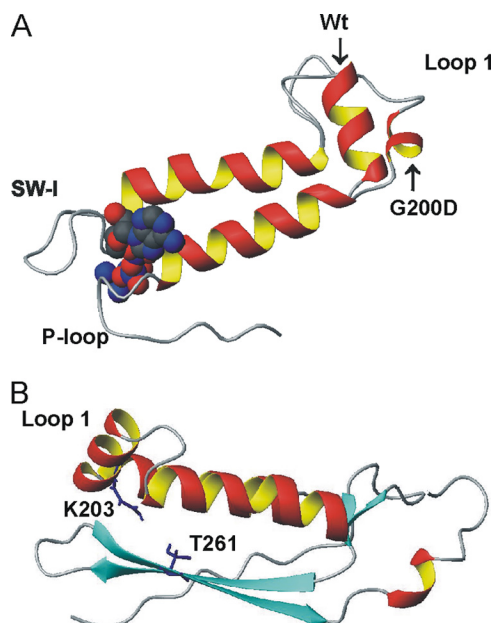


FIGURE 8. Homology models of $S1^{G200D}$ (A) and $S1^{A261T}$ (B) suggest a role for loop 1. *A*, overlay of the loop 1 area of homology models of wild-type S1 (Wt) and $S1^{G200D}$ (built using pre-powerstroke scallop myosin (PDB code 1qvi) as template) showing a helical structure of loop 1 for wild type, which is disrupted in $S1^{G200D}$. The bound nucleotide is shown as solid spheres, and switch 1 (SW-I) and the phosphate binding loop (P-loop) are also indicated. *B*, loop 1 area of $S1^{A261T}$ shows a wild type-like helical structure for loop 1. The conserved loop 1 residue Lys²⁰³ can interact with Thr²⁶¹, which is located on β^7 . The altered structure of loop 1 may affect its flexibility and ultimately change ADP release rate for the mutants, with faster release for $S1^{G200D}$ (less ordered loop 1 structure) and slower release for $S1^{A261T}$ (more rigid loop 1 structure).

are less profound. For the rigor state, the models predict a disordered loop 1 for all three S1s. For the post-rigor state, loop 1 is predicted to contain a small helix, with $S1^{A261T}$ being the longest (three turns) and $S1^{G200D}$ the shortest (one turn) (not shown).

DISCUSSION

We investigated the steady-state and transient kinetics of two transducer mutant myosin S1 fragments that 1) yield normal morphology (A261T) or hypercontraction (G200D) in the IFM (2, 8); 2) can suppress (A261T) or enhance (G200D) the hypercontraction phenotype caused by a troponin I defect (TnI-A116V); and 3) can also induce specific phenotypes in the *Drosophila* heart (7). This is summarized in Table 1. The data show that the two point mutations have an opposite effect on the enzymatic activity of the S1 as compared with wild type. $S1^{A261T}$ is less active (reduced basal ATPase and V_{max}/K_m , higher ADP affinity for S1 (K_D) and actin·S1 (K_{AD}), and reduced ATP-induced dissociation of actin·S1 (K_{1k+2})), whereas $S1^{G200D}$ shows an increase in enzymatic activity (enhanced basal ATPase and V_{max}/K_m and reduced ADP affinity for both S1 (K_D) and actin·S1 (K_{AD})). These results agree with and substantially extend previous work on the same mutations in full-length myosin (7). By defining the biochemical parameters that differ between the two transducer mutants, our results provide new insights into the molecular mechanisms that cause different phenotypes for these mutants on their own and in combination with the *held-up*² TnI mutation.

Point Mutants of *Drosophila* Muscle Myosin

There is an emerging consensus that in the case of HCM (of which RCM is a subset), mutant contractile proteins result in increased contractility or motor function and are usually associated with an increase in the calcium sensitivity of contraction. In contrast, mutations that result in DCM yield decreased contractility or motor function that is often associated with a decrease in calcium sensitivity (9, 23–27). Our results are consistent with the induced cardiac phenotypes because actin·S1^{A261T} has decreased activity and results in a DCM phenotype (dilated), whereas actin·S1^{G200D} results in increased activity, and this mutation causes an RCM phenotype (restrictive). Our data also show for the first time that the affinity of S1·ADP for actin is affected in opposite ways with the RCM mutant having very tight actin affinity and the DCM mutant showing weaker actin affinity as compared with wild type. Because these particular mutations affect the transducer region, which provides a communication pathway between the actin and nucleotide binding sites (11), the changes in transducer structure might be predicted to have effects on the actin affinity of S1 in the presence of ADP. However, note that although residues Ala²⁶¹ and Gly²⁰⁰ and the transducer region are common to both the cardiac and the IFI myosin isoforms, there are differences in other domains of the myosin head between the IFI and cardiac myosin isoforms (28). Thus the IFI isoform can model the heart isoforms, but is not identical.

Can our results help explain the interaction between the mutant myosins characterized here and the TnI *held-up*² mutation? The regulation of muscle contraction by troponin relies, at one level, on a competition between TnI and myosin for binding sites on actin. In the absence of calcium, TnI binds actin more tightly than myosin; in the presence of calcium, the TnI interaction is weakened, and now myosin binds more tightly. *In vitro* motility assays of regulated thin filaments showed that the *hdp*² mutant troponin I caused activation of motility at lower calcium concentrations than wild type (29, 30). If the *held-up*² phenotype is caused by the A116V TnI mutation weakening the inhibitory interaction of TnI with actin, then a mutation in myosin that weakens its interaction with actin could bring the two affinities back into balance. The AM·ADP complex is expected to be a significant force-holding state in the cross-bridge cycle. Alterations in the affinity of AM·ADP for actin could alter the ability of the AM·ADP state to compete with TnI for binding to actin. Our estimate of K_{DA} for S1^{A261T} (weaker actin binding than wild-type IFI) is consistent with this prediction and with this mutation operating as a suppressor of the *held-up*² phenotype. In contrast, S1^{G200D} has a higher affinity of S1·ADP for actin, and the G200D mutation is expected to be able to activate more readily than wild-type myosin. In addition to the direct effect of competition between TnI and myosin, a more strongly bound myosin would, through the cooperativity in the thin filament, enhance the affinity of the Tn complex for calcium (31). This, in combination with *held-up*², will result in activation at very low calcium concentrations. This can explain the lethality observed when these two mutations are placed within the same organism, where muscles essential for viability are constitutively activated. These characteristics of the G200D activating more readily and A261T activating less well are also

consistent with alterations in calcium sensitivity associated with the DCM and RCM cardiac defects.

Another characteristic change produced in myosin by the two mutations is the change in the *in vitro* motility. The velocity was enhanced by 16% for G200D and reduced by 55% for A261T (7). The velocity at which myosin moves actin in a motility assay and the maximum speed of muscle fiber shortening are normally considered to be limited by the rate constant for cross-bridge detachment after completion of the working stroke (32–34). For fast myosins, cross-bridge detachment is usually limited by ATP binding, whereas for slower myosins, ADP release is rate-limiting. However, for *Drosophila* IFM fibers at saturating ATP (20 mM), the rate-limiting step of fiber shortening is inorganic phosphate release (35). Because IFM fibers have a very weak affinity for ATP, at the ATP concentration used for the motility assays (2 mM), ATP binding could be rate-limiting instead of phosphate release. However, *in vitro* motility data are collected under unloaded conditions, whereas fiber data represent loaded conditions, which could result in different rate-limiting steps. For the IFM, as for fast mammalian muscle, the ADP release is expected to be much too fast to limit the velocity, and this remains true for the two mutant myosins. Here we report that the second-order rate constant (K_1k_{+2}) for ATP-induced dissociation of actin·S1^{A261T} is reduced to about 60% of the value of the IFI. This is similar to the 55% reduction in the velocity of *in vitro* motility assays. In contrast, there is no significant difference between the rate constant for ATP-induced dissociation of actin·S1^{G200D} and wild type and only a 16% difference in the *in vitro* motility velocity.

The homology models suggest a possible loop 1-based mechanism for how the two mutations affect myosin kinetics in opposite ways. The rate constant of ADP release (k_{-AD} and hence K_{AD}) has been correlated with the size and flexibility of loop 1, with the larger and more flexible loops giving higher release rate constants (36). Loop 1 is also one of the key players in transducer region function, and its importance has been emphasized by Houdusse and co-workers (11) who called the transducer region “loop 1 tuning elements.” Although the surface loop 1 is not usually seen in myosin crystal structures because of its inherent flexibility, our homology models do predict differences in the apparent flexibility of the loop in the three myosins. For wild type, going from near-rigor to post-rigor to pre-powerstroke states, the models predict an increase in the probability of a helical structure, implying less flexibility for the loop in the pre-powerstroke state. A similar trend is seen for the three structures of each of the two mutants, with A261T tending to have more helix in loop 1 in each case and G200D less. The models suggest that for wild-type myosin in the most stable (pre-powerstroke) state, loop 1 is largely an α -helix that starts at Gly²⁰⁰. For S1^{G200D}, the introduction of the larger Asp side chain appears to disrupt the start of the helical structure, resulting in a more flexible loop that may lead to faster ADP release rates. In the case of S1^{A261T}, loop 1 may become less flexible due to the interaction between Lys²⁰³ (in loop 1) and Thr²⁶¹, resulting in slower ADP release.

In summary, this study of the two myosin point mutations reveals characteristics that are compatible with the observed IFM and cardiac phenotypes. In addition, the changes in the

two mutant S1s provide an explanation of the ability of A261T to suppress the *held-up*² phenotype as well as the lethality of the G200D mutation in combination with *held-up*². The opposing biochemical defects we uncovered provide insight into how mutations within the same gene can result in disparate mutant muscle phenotypes.

Acknowledgments—We acknowledge the excellent technical assistance of Anju Melkani (myosin preparation) and Sam Lynn (co-sedimentation). We thank Dr. A. Cammarato for reading the manuscript and providing comments.

REFERENCES

- Odrionitz, F., and Kollmar, M. (2007) *Genome Biol.* **8**, R196
- O'Connell, C. B., Tyska, M. J., and Mooseker, M. S. (2007) *Biochim. Biophys. Acta* **1773**, 615–630
- Geeves, M. A., Fedorov, R., and Manstein, D. J. (2005) *Cell. Mol. Life Sci.* **62**, 1462–1477
- Seidman, J. G., and Seidman, C. (2001) *Cell* **104**, 557–567
- Wolf, M. J., Amrein, H., Izatt, J. A., Choma, M. A., Reedy, M. C., and Rockman, H. A. (2006) *Proc. Natl. Acad. Sci. U.S.A.* **103**, 1394–1399
- Ocorr, K. A., Crawley, T., Gibson, G., and Bodmer, R. (2007) *PLoS One* **2**, e601
- Cammarato, A., Dambacher, C. M., Knowles, A. F., Kronert, W. A., Bodmer, R., Ocorr, K., and Bernstein, S. I. (2008) *Mol. Biol. Cell* **19**, 553–562
- Kronert, W. A., Acebes, A., Ferrús, A., and Bernstein, S. I. (1999) *J. Cell Biol.* **144**, 989–1000
- Robinson, P., Griffiths, P. J., Watkins, H., and Redwood, C. S. (2007) *Circ. Res.* **101**, 1266–1273
- Dweck, D., Hus, N., and Potter, J. D. (2008) *J. Biol. Chem.* **283**, 33119–33128
- Coureau, P. D., Sweeney, H. L., and Houdusse, A. (2004) *EMBO J.* **23**, 4527–4537
- Swank, D. M., Knowles, A. F., Kronert, W. A., Suggs, J. A., Morrill, G. E., Nikkhoy, M., Manipon, G. G., and Bernstein, S. I. (2003) *J. Biol. Chem.* **278**, 17475–17482
- Nanni, L., Pieroni, M., Chimenti, C., Simionati, B., Zimbello, R., Maseri, A., Frustaci, A., and Lanfranchi, G. (2003) *Biochem. Biophys. Res. Commun.* **309**, 391–398
- Miller, B. M., Nyitrai, M., Bernstein, S. I., and Geeves, M. A. (2003) *J. Biol. Chem.* **278**, 50293–50300
- Bloemink, M. J., Dambacher, C. M., Knowles, A. F., Melkani, G. C., Geeves, M. A., and Bernstein, S. I. (2009) *J. Mol. Biol.* **389**, 707–721
- Webb, M. R., Reid, G. P., Munasinghe, V. R., and Corrie, J. E. (2004) *Biochemistry* **43**, 14463–14471
- Webb, M. R., and Corrie, J. E. T. (2001) *Biophys. J.* **81**, 1562–1569
- Weiss, S., Chizhov, I., and Geeves, M. A. (2000) *J. Muscle Res. Cell Motil.* **21**, 423–432
- Miller, B. M., Bloemink, M. J., Nyitrai, M., Bernstein, S. I., and Geeves, M. A. (2007) *J. Mol. Biol.* **368**, 1051–1066
- Arnold, K., Bordoli, L., Kopp, J., and Schwede, T. (2006) *Bioinformatics* **22**, 195–201
- Schwede, T., Kopp, J., Guex, N., and Peitsch, M. C. (2003) *Nucleic Acids Res.* **31**, 3381–3385
- Clark, R. J., Nyitrai, M., Webb, M. R., and Geeves, M. A. (2003) *J. Muscle Res. Cell Motil.* **24**, 315–321
- Schmitt, J. P., Debold, E. P., Ahmad, F., Armstrong, A., Frederico, A., Conner, D. A., Mende, U., Lohse, M. J., Warshaw, D., Seidman, C. E., and Seidman, J. G. (2006) *Proc. Natl. Acad. Sci. U.S.A.* **103**, 14525–14530
- Lakdawala, N. K., Dellefave, L., Redwood, C. S., Sparks, E., Cirino, A. L., Depalma, S., Colan, S. D., Funke, B., Zimmerman, R. S., Robinson, P., Watkins, H., Seidman, C. E., Seidman, J. G., McNally, E. M., and Ho, C. Y. (2010) *J. Am. Coll. Cardiol.* **55**, 320–329
- Marston, S. B. (2011) *J. Cardiovasc. Transl. Res.* **4**, 245–255
- Palmer, B. M., Fishbaugher, D. E., Schmitt, J. P., Wang, Y., Alpert, N. R., Seidman, C. E., Seidman, J. G., VanBuren, P., and Maughan, D. W. (2004) *Am. J. Physiol. Heart Circ. Physiol.* **287**, H91–H99
- Debold, E. P., Schmitt, J. P., Patlak, J. B., Beck, S. E., Moore, J. R., Seidman, J. G., Seidman, C., and Warshaw, D. M. (2007) *Am. J. Physiol. Heart Circ. Physiol.* **293**, H284–H291
- Cammarato, A., Ahrens, C. H., Alayari, N. N., Qeli, E., Rucker, J., Reedy, M. C., Zmasek, C. M., Gucek, M., Cole, R. N., Van Eyk, J. E., Bodmer, R., O'Rourke, B., Bernstein, S. I., and Foster, D. B. (2011) *PLoS ONE* **6**, e18497
- Vikhorev, P. G., Vikhoreva, N. N., Cammarato, A., and Sparrow, J. C. (2010) *J. Muscle Res. Cell Motil.* **31**, 171–179
- Lin, N., Badie, N., Yu, L., Abraham, D., Cheng, H., Bursac, N., Rockman, H. A., and Wolf, M. J. (2011) *Circ. Res.* **108**, 1306–1315
- Gordon, A. M., Homsher, E., and Regnier, M. (2000) *Physiol. Rev.* **80**, 853–924
- Siemankowski, R. F., Wiseman, M. O., and White, H. D. (1985) *Proc. Natl. Acad. Sci. U.S.A.* **82**, 658–662
- Nyitrai, M., Rossi, R., Adamek, N., Pellegrino, M. A., Bottinelli, R., and Geeves, M. A. (2006) *J. Mol. Biol.* **355**, 432–442
- Baker, J. E., Brosseau, C., Joel, P. B., and Warshaw, D. M. (2002) *Biophys. J.* **82**, 2134–2147
- Swank, D. M., Vishnudas, V. K., and Maughan, D. W. (2006) *Proc. Natl. Acad. Sci. U.S.A.* **103**, 17543–17547
- Sweeney, H. L., Rosenfeld, S. S., Brown, F., Faust, L., Smith, J., Xing, J., Stein, L. A., and Sellers, J. R. (1998) *J. Biol. Chem.* **273**, 6262–6270